Radio Science, Volume 28, Number 6, Pages 1003–1018, November–December 1993

Ground-based measurement of gradients in the "wet" radio refractivity of air

James L. Davis[1], Gunnar Elgered[2], Arthur E. Niell[3], and Clara E. Kuehn[4]

(Received April 7, 1992; revised June 30, 1993; accepted June 30, 1993.)

We have used a ground-based microwave radiometer, known as a water vapor radiometer, to investigate the local spatial and temporal variation of the wet propagation delay for a site on the west coast of Sweden. The data were obtained from a wide range of azimuths and from elevation angles greater than 23.6° (air mass 2.5). Visual inspection of the data suggested a simple "cosine azimuth" variation, implying that a first-order gradient model was required. This model was adequate for short time spans up to approximately 15 min, but significant temporal variations in the gradient suggested to us that we include gradient rate terms. The resulting six-parameter model has proven adequate (rms delay residual ~1 mm) for up to 30 min of data. Assuming a simple exponential profile for the wet refractivity gradient, the estimated gradient parameters imply average surface wet-refractivity horizontal gradients of order of 0.1–1 N km^{-1}. These gradients are larger, by 1–2 orders of magnitude, than gradients determined by others by averaging over long (~100-km) distances. This result implies that for applications that are sensitive to local gradients, such as wet propagation-delay models for radio-interferometric geodetic studies, the use of meteorological data from widely spread stations may be inadequate. The gradient model presented here is inadequate for times longer than about 30 min, even if no gradients are present, because of the complicated stochastic like temporal behavior of the wet atmosphere. When gradients are present, they can change magnitude by ~50% over 10–15 min. Nevertheless, our ability to fit the radiometer data implies that on timescales <30 min and for elevation angles >23.6°, the local structure of the wet atmosphere can be described with a simple model. (The model is not limited to this range of elevation angles in principle.) The estimated gradient and gradient rate vectors have preferred directions, which indicates a prevailing structure in the three-dimensional temperature and humidity fields, possibly related to systematic behavior in large-scale weather systems and/or the local air-land-sea interaction at this site.

INTRODUCTION

The neutral atmosphere refracts incoming radio signals, increasing the travel time for those signals. This delay is a source of error for measurement techniques that rely on the timing of the arrival of signals of extraterrestrial origin at widely separated points on the Earth. The most accurate of these techniques for the determination of relative position and other geophysical information is currently very long baseline interferometry (VLBI). The primary observable of geodetic VLBI is the wideband group delay, which for current systems has a measurement uncertainty of ~30 ps or less.

In order to account for the atmospheric propagation effects of the group delay, some combination of modeling and estimation is usually used. One of the least tractable problems is the effect of water vapor on radio propagation. Because humidity at altitude is not generally well correlated with surface humidity [Reber and Swope, 1972], models for the "wet delay" based on measured surface quantities are inaccurate [Elgered, 1982]. The problem is complicated by the extreme and rapid time variability of the water-vapor distribution, and hence the wet delay, at any site. Recently, stochastic filtering techniques have been successfully applied to the analysis of VLBI group delay data [Herring et al., 1990].

Another method undergoing development for estimation of the wet delay is based on ground-based microwave radiometry [Resch, 1984; Elgered et al., 1991]. A radiometer used specifically for the purpose of estimating the wet delay is known as a "water vapor radiometer," or WVR. Were this method to

[1]Harvard-Smithsonian Center for Astrophysics, Cambridge, Massachusetts.

[2]Onsala Space Observatory, Chalmers University of Technology, Onsala, Sweden.

[3]Haystack Observatory, Massachusetts Institute of Technology, Westford, Massachusetts.

[4]Interferometrics, Incorporated, Vienna, Virginia.

Paper number 93RS01917.
0048-6604/93/93RS-01917$08.00

prove accurate enough, its use could improve the accuracy with which site positions (especially, the vertical coordinate) are determined. Another potential advantage of such a method is that it could sense spatial, that is, horizontal, variations in the propagation delay. For example, Dixon and Kornreich Wolf [1990] noted that radiometrically determined values for the wet delay exhibited a systematic but time-variable difference when the WVR was consecutively pointed in diametrically opposite azimuths. The maximum size of the difference (referenced to an elevation of 30°) was ~20 mm.

This paper describes our investigation of horizontal variations in the radio refractivity of air using WVR data. In the following sections we first describe the WVR data used for the analysis. We then develop a simple model for the horizontal variations suggested by visual examination of the WVR data and use the WVR data to estimate parameters of the model. Finally, we discuss the implications of our results for the instrumental calibration of the WVR and for estimating horizontal variations in the hydrostatic (mainly dry) component of the atmospheric propagation delay.

WATER VAPOR RADIOMETERS

In this section, we briefly discuss the determination of the wet propagation delay from radiometric data and present examples of wet delay estimates. The subsection on WVR algorithms can be skipped by those familiar with this topic.

WVRs used

A water vapor radiometer is a multichannel microwave radiometer. When the WVR has only two channels, the frequency band of one is centered near (but slightly off center from) the 22-GHz rotational line of water vapor, whereas the frequency band of the other channel is located well off the line (typically near 31 GHz). The operating characteristics of the two WVRs used in this study are given in Elgered et al. [1991]. The first WVR, ASTRID, is a dual-frequency (21.0 and 31.4 GHz) WVR located permanently at the Onsala Space Observatory on the Råö peninsula on the west coast of Sweden (Figure 1). J03, the other WVR, has three channels, but for this study we will make use of only channels 1 and 3 (20.7 and 31.4 GHz). J03 was brought to the Onsala site in June and July 1988 for a side-by-side comparison with ASTRID. The J03 data used here were obtained during this period.

WVR algorithms

Each channel of each WVR is used to measure (independently) the emission from the sky in the frequency band associated with that channel. Each WVR is designed to output a digital signal proportional to the observed sky brightness temperature T_b, which is related to the optical depth τ_∞ (in the direction the WVR is pointed) by the equation of radiative transfer [Chandrasekhar, 1960]:

$$T_b = T_{bg}e^{-\tau_\infty} + \int_0^\infty ds\, T(s)\alpha(s)e^{-\tau(s)} \qquad (1)$$

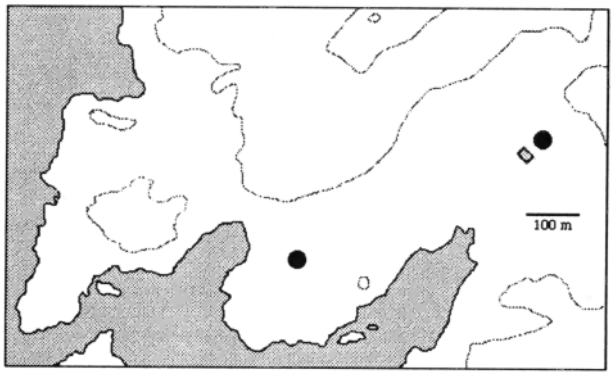

Fig. 1. Map of the Onsala Space Observatory area [after Johansson, 1992]. The black circle to the northeast is the radome containing the 20-m radio telescope. The circle to the southwest is the 25.6-m radio telescope (no radome). The rectangle represents the position of the ASTRID WVR. (The figures representing the telescopes and the WVR are not drawn to scale.) The elevation contours (dotted lines) are shown for 10-m intervals. The shaded area represents ocean.

where T_{bg} is the "background temperature" (i.e., due to emission from outside the Earth's atmosphere). In the frequency band relevant to WVRs, T_{bg} is due primarily to the cosmic background radiation. $T(s)$ is the physical temperature of the atmosphere along the integration path s, and $\alpha(s)$ is the (composite) attenuation coefficient (emissivity) of water vapor, liquid water, and oxygen. The parameter $\tau(s)$ is the opacity from the ground to the point s:

$$\tau(s) = \int_0^s ds'\, \alpha(s') \qquad (2)$$

For $s \to \infty$, the opacity is written as τ_∞.

Examining (1) and (2), one can make several observations regarding the use of the WVR observables T_b for studying variations in the wet refractive index. The brightness temperature is not a linear function of the integrated atmospheric water vapor quantity but saturates for $\tau_\infty \not\ll 1$; T_b is sensitive to emission by oxygen and liquid water as well as to water vapor; and T_b depends on the combined emissivity of these constituents, not their refractive index.

The problem of linearity is solved by using not T_b directly but by solving (1) for τ_∞. From (2), we can see that this quantity is linear in the integrated emissivity. Alternatively, some investigators use the "linearized brightness temperature" [Wu, 1979].

For water droplets small with respect to the WVR wavelengths ($\ll$ 10 mm), the emissivity of liquid water has a frequency-squared dependence [Staelin, 1966; Liebe et al., 1991]. Therefore, in order to eliminate the influence of liquid water, the "on-line" and "off-line" opacities are combined to create a liquid-free observable [e.g., Wu, 1979]. The remaining contribution of oxygen is small and can be modeled using

values for pressure and temperature at the surface [Wu, 1979].

In order to use radiometry for studies of the refractive index, one seeks a relationship between the contribution of water vapor to the absorption and the refractive index. There is, in fact, no unique relationship, but in one method one expresses the water vapor absorption α_v as a linear function of the wet refractivity N_v:

$$\alpha_v(s) = 10^{-6} W(s)^{-1} N_v(s) \tag{3}$$

where $W(s)$ is a "weighting function" (described further below). The wet refractivity is the contribution due to water vapor to the total refractivity N, defined in terms of the refractive index n by

$$N(s) = 10^6 [n(s) - 1] \tag{4}$$

The weighting function approach described by (3) is successful primarily because both α_v and N_v vary (approximately) linearly with the density of water vapor. (See, e.g., Staelin [1966] for expressions for α_v and Boudouris [1963] for those for N_v. Also, see Liebe [1989] for a discussion of higher-order terms.) Thus the weighting function $W(s)$ has a weak dependence on the density of water vapor and therefore does not vary much from day to day or spatially. Integrating both sides of (3) along the path through the atmosphere in the direction the WVR is pointing yields

$$\begin{aligned} \tau_v &= 10^{-6} \int_0^\infty ds\ W(s)^{-1} N_v(s) \\ &= 10^{-6} \overline{W}^{-1} \int_0^\infty ds\ N_v(s) \\ &= \overline{W}^{-1} \Delta L \end{aligned} \tag{5}$$

where the bar indicates average, in this case weighted by the wet refractivity, and ΔL is the "wet delay" [e.g., Davis, 1986].

In practice, (5) is not used directly. As mentioned above, a liquid-free observable is first formed. The resulting expression looks like (5), except the left-hand side has a liquid-free linear combination of the total opacities obtained at different frequencies, and $\overline{W}$ becomes a dual-frequency weighting function [Wu, 1979]. The refractivity, and hence the wet delay, have no significant dependence on frequency in the range 0–50 GHz [Liebe, 1985, 1987].

In order to determine values for $\overline{W}$, radiosonde data are used. One needs expressions for the absorption and refractivity as a function of pressure, temperature, humidity, and (in the case of absorption) frequency. Such expressions can be found in, for example, Liebe [1985, 1987]. Linear regression is applied to radiosonde data for a given site to determine the values for $\overline{W}$ as well as its dependence upon surface temperature and pressure. The best retrieval algorithms devised yield root-mean-square (rms) errors of 1–2 mm for the zenith direction using four years of radiosonde observations obtained twice per day [Johansson et al., 1987].

A source of error not revealed by the regression rms arises from deficiencies in the expressions for the refractivity and absorption coefficients. The uncertainty due to errors in the refractivity formula is less than 1% [Davis et al., 1985]. On the basis of comparison of different expressions available, Elgered et al. [1991] estimated that the uncertainty in estimated wet delay due to errors in the expressions for the absorptions is about 5% of the wet delay. In this study we are interested in variations of the wet delay, so the effect should be scaled; that is, the uncertainty in the variations will be about 5% of the total variation.

WVR data: An example

Figure 2 shows data obtained from the ASTRID WVR on July 11, 1988. The estimates of the wet delay are traditionally given in units of distance, that is, the time delay multiplied by the speed of light in vacuum. The data appear to be separated into groups, a phenomenon related to the manner in which the data were obtained. The WVR was performing azimuth scans, with an observation obtained at azimuths of 100°, 110°, ..., 350°, at a given elevation angle (around 30°). No observations could be obtained between azimuths of 0° and 100° at this elevation angle because a nearby large radome occludes the sky (Figure 1). Four "tip curves" were also performed at azimuths of 100°, 180°, 270°, and 350°, but the data from these are not shown in the figures for clarity. The estimates of wet delay in this and other plots will be given in "equivalent zenith delay," that is, divided by the mapping function (see below). This will allow us to compare variations for data obtained at different elevation angles.

Also shown are data obtained from the J03 WVR during the same time span. The two instruments were not synchronized, so they did not observe in the same direction at the same epoch. The J03 data were obtained at approximately the same elevation angle, but at different times, and using azimuth steps of 30°. No bias has been removed from either series of estimates. Figure 2 is meant to be illustrative; a more thorough analysis indicates that agreement of this type is typical [Kuehn et al., 1993]. We have computed an overall correlation of 0.6 between estimated gradient parameters. Käll [1991] has compared in more detail several thousand observations from the two WVRs for July 21–22, 1988, and has computed correlation coefficients of 0.7–0.8 for the gradient parameters estimated nearly simultaneously from the two instruments. This correlation argues against the azimuthal variations being due to instrumental tilt, especially since the gradient parameters vary with time. (An instrumental tilt of 1° would cause a maximum error in the equivalent zenith wet delay of ±13 mm at an elevation angle of 20° and would be constant in time.)

From Figure 2, it is apparent that during the time interval of the plot there was an overall rapid decrease in the wet delay of ~80 mm in 4 hours. There is also a large amount of variation within each scan. In Figure 3*a*, we show two of the scans expanded so that the periodic nature of the variation can be seen. In Figure 3*b*, we plot the data from these same two

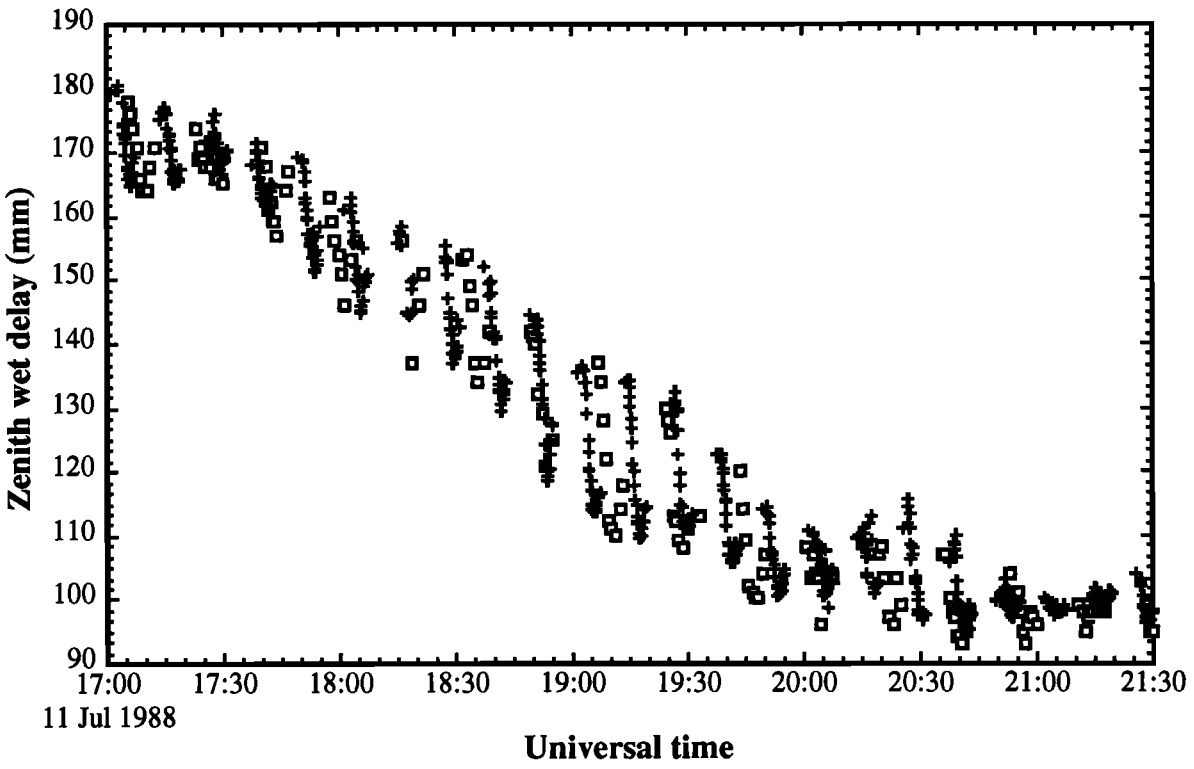

Fig. 2. WVR determinations of the equivalent wet zenith delay for the ASTRID WVR (plus signs) and for the J03 WVR (squares). The WVRs were executing a series of commands requiring them to perform repeatedly a scan in azimuth for a constant elevation angle. Between azimuth scans a tip curve in elevation was performed. The tip curve data are not shown in this figure in order to clarify the effects of a horizontal refractivity gradient on the azimuth scan data. Error bars are not shown on this figure, but they are approximately ±1 mm (based on residuals to tip curve analyses).

scans, except we show the delay as a function of the azimuth of the observation.

GRADIENT MODEL

The horizontal variation of water vapor is potentially complicated. For example, clouds could give rise to clumps in the water vapor distribution. Nevertheless, the cosinelike behavior of the wet delay estimates in Figure 3*b* suggests that a simple gradient model might be adequate.

Let us obtain an expression for the wet refractivity by performing a first-order Taylor expansion of the refractivity at altitude z with respect to the horizontal position vector $\vec{x}$ measured from the site:

$$N(\vec{x}, z; t) = N_o(z; t) + \vec{\xi}(z; t) \cdot \vec{x} \tag{6}$$

where $\vec{\xi}$ is the horizontal gradient of refractivity at $\vec{x} = 0$:

$$\xi_i(z; t) = \left.\frac{\partial N(\vec{x}, z; t)}{\partial x_i}\right|_{\vec{x}=0} \tag{7}$$

In (7), the subscript i refers to the ith component of $\vec{x}$: x_1 for east and x_2 for north. The subscript circle on the first term on the right-hand side of (6) indicates $\vec{x} = 0$. We have dropped the previously used subscript v (for vapor) for clarity.

The wet delay in any direction is given by the integration of (6) along the path s in that direction. Parametrized by elevation ϵ and azimuth ϕ (and dropping the explicit time dependence), this integration yields

$$\begin{aligned}\Delta L(\epsilon, \phi) &= 10^{-6} \int_0^\infty ds\ N(s) \\ &= 10^{-6} \int_0^\infty ds\ N_o(z) + 10^{-6} \int_0^\infty ds\ \vec{\xi}(z) \cdot \vec{x} \\ &= \Delta L_o(\epsilon) + 10^{-6} \int_0^\infty ds\ \vec{\xi}(z) \cdot \vec{x}\end{aligned} \tag{8}$$

where ΔL_o is the wet delay for zero gradient. In (8), we have ignored the difference in the integration paths for the gradient and no-gradient cases. (The error associated with this assumption is explored in the discussion section.)

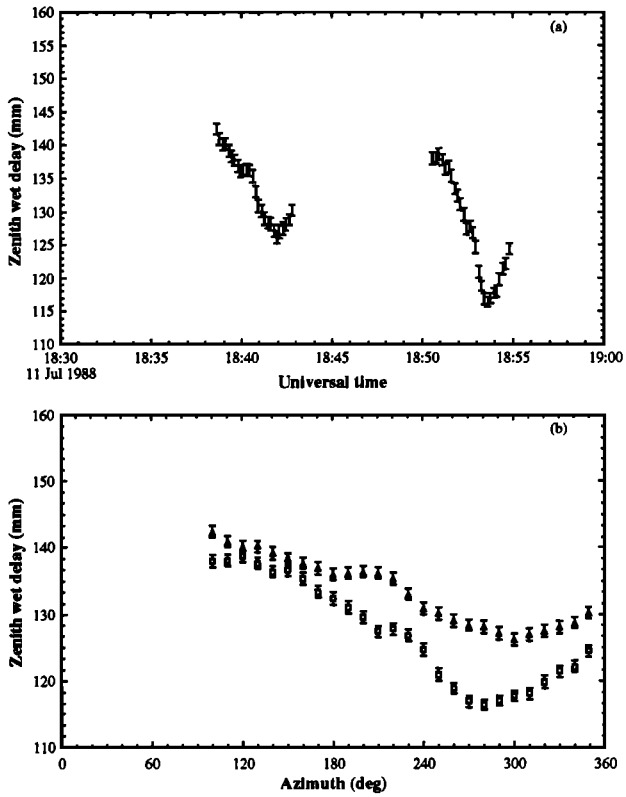

Fig. 3. Two of the azimuth scans (ASTRID data) from Figure 2. (*a*) Equivalent wet zenith delay versus time. (*b*) The same data plotted against azimuth angle. The triangles represent the earlier data, and the squares represent the later data.

It is convenient here to introduce the concept of a mapping function [e.g., Davis et al., 1985]. The mapping function expresses the elevation angle dependence of the propagation delay. In the absence of horizontal refractivity variations (i.e., when the wet delay has no dependence upon azimuth), the mapping function $m_o(\epsilon)$ is defined by

$$\Delta L_o(\epsilon) \equiv \Delta L^z m_o(\epsilon) \tag{9}$$

where ΔL^z is the "zenith delay," that is, the wet delay in the zenith direction. Again, the nought subscript on m in (9) indicates the zero-gradient function. The zenith delay needs no subscript because, by definition, $\vec{x} = 0$ for the zenith direction, and from (8) one sees immediately that $\Delta L^z = \Delta L^z_o$.

As an extension to (9) one can define an azimuth-dependent mapping function which takes gradients into account (continuing to ignore the difference in ray paths for the gradient and no-gradient case):

$$\Delta L(\epsilon, \phi) = \Delta L^z m(\epsilon, \phi) \tag{10}$$

Using (9) and (10), one can write (8) in terms of mapping functions as

$$m(\epsilon, \phi) = m_o(\epsilon) + 10^{-6} \int_0^\infty ds\ \vec{\zeta}(z) \cdot \vec{x} \tag{11}$$

where $\vec{\zeta}(z) = \vec{\xi}(z)/\Delta L^z$. Thus a gradient causes the mapping function to differ from the zero-gradient mapping function by an additive term. Denoting this term δm (i.e., $m = m_o + \delta m$), one can get an estimate for this function from (11) using the following relations:

$$\begin{aligned} \vec{x}(\epsilon, \phi) &\simeq z \cot \epsilon' (\cos\phi \hat{n} + \sin\phi \hat{e}) \\ \vec{\zeta}(z) &= \zeta_n \hat{n} + \zeta_e \hat{e} \\ ds &\simeq dz\ m_o(\epsilon) \end{aligned} \tag{12}$$

where n refers to north and e to east (and $\hat{n}$ and $\hat{e}$ to unit vectors in those directions). The quantity ϵ' is the "refracted" elevation angle and will be discussed below; however, the difference between ϵ and ϵ' is significant only for low elevation angles. Using the relationships in (12), one obtains

$$\begin{aligned} \delta m(\epsilon, \phi) &\simeq 10^{-6} m_o(\epsilon) \cot \epsilon' \\ &\quad \times \left[\cos\phi \int_0^\infty dz\ z\ \zeta_n(z) + \sin\phi \int_0^\infty dz\ z\ \zeta_e(z) \right] \\ &= m_o(\epsilon) \cot \epsilon' \left[Z_n \cos\phi + Z_e \sin\phi \right] \end{aligned} \tag{13}$$

where

$$\vec{Z} = 10^{-6} \int_0^\infty dz\ z\ \vec{\zeta}(z) \tag{14}$$

In this paper, the upper case symbols (Z and Ξ, introduced later) symbolize integrated gradients; the gradients themselves are symbolized by lower case symbols (ζ and ξ). The upper and lower case zeta (Z and ζ) are used to distinguish the quantities which are "normalized" (by the zenith wet delay) from the unnormalized quantities, represented by upper and lower case xi (Ξ and ξ). These relationships and the definitions of other quantities are given in Table 1.

From (13) one can see that δm has the azimuth dependence one would expect from a first-order model, that is, one that arises directly from the $\vec{\xi} \cdot \vec{x}$ term in (6). Its elevation angle dependence is the product of two terms. The dependence on m_o occurs because the distance along the integration path is greater for lower elevation angles, as usual. The cotangent term arises because, for lower elevation angles, the signal passes through atmosphere present at a greater horizontal distance from the site, thereby encountering a greater refractivity difference (since our original model had refractivity varying linearly with horizontal distance).

By convention, the mapping function is defined in such a way as to depend on the true, that is, unrefracted, elevation angle ϵ of the source [Davis et al., 1985]. The cotangent term, however, depends on the refracted elevation angle ϵ', since that angle defines the path of the ray through the troposphere, where water vapor is present, and where water vapor gradients must therefore occur. (We will assume that the bending in azimuth due to horizontal gradients is negligible, so $\phi = \phi'$.) The true and refracted elevation angles are related by

TABLE 1. Formulas and Definitions Used

Quantity	Definition
Basic Terms	
Horizontal position vector[a]	$\vec{x}$
Atmospheric altitude	z
Refractivity	$N(\vec{x}, z)$
Elevation angle	ϵ
Azimuth	ϕ
Wind velocity[b]	$\vec{v}(z)$
Slant path differential[c]	ds
Wet Delay Definitions	
Wet delay	$\Delta L(\epsilon, \phi) = 10^{-6} \int_0^\infty ds\ N(\vec{x}, z)$
Wet delay, no gradients	$\Delta L_o(\epsilon) = 10^{-6} \int_0^\infty ds\ \ N(\vec{x}, z)\|_{\vec{x}=0}$
Zenith delay	$\Delta L^z = 10^{-6} \int_0^\infty dz\ \ N(\vec{x}, z)\|_{\vec{x}=0}$
Gradients	
Refractivity gradient[d]	$\xi_i(z) = \frac{\partial N(\vec{x},z)}{\partial x_i}\Big\|_{\vec{x}=0}$
Delay gradient	$\Xi_i = 10^{-6} \int_0^\infty dz\ z\ \xi_i(z)$
Normalized Gradients (for Mapping Functions)	
Normalized refractivity gradient	$\zeta_i(z) = \xi_i(z)/\Delta L^z$
Normalized delay gradient	$Z_i = \Xi_i/\Delta L^z$
Mapping Functions	
Wet mapping function	$m(\epsilon, \phi) = \Delta L(\epsilon, \phi)/\Delta L^z$
Wet mapping function (no gradients)	$m_o(\epsilon) = \Delta L_o(\epsilon)/\Delta L^z$
Miscellaneous	
Zenith delay rate	$V_L = 10^{-6} \int_0^\infty dz\ \vec{\xi}(z) \cdot \vec{v}(z)$

[a]The coordinate convention is x_1 is east, x_2 north.

[b]Assumed to be parallel to surface of earth.

[c]The integration path is in the direction of interest. When that direction is vertical (the zenith direction), ds is written as dz.

[d]Horizontal gradient; $i = 1, 2$ (east, north).

$$\epsilon' \equiv \epsilon + \delta\epsilon(\epsilon) \tag{15}$$

An approximate expression for $\delta\epsilon$, accurate to about 10% above $\epsilon = 5°$ [Bean and Dutton, 1966], is

$$\delta\epsilon \simeq 10^{-6} N_s \cot\epsilon \tag{16}$$

where N_s is the total surface refractivity and $\delta\epsilon$ is given in radians. For a typical sea level value for N_s of ~300, $\delta\epsilon \simeq 0.2°$ for $\epsilon = 5°$. We compared values calculated for $\delta\epsilon$ using (16) with values determined from a ray-tracing program and found that the error in (16) is less than 0.03° for $\epsilon = 5°$, and less than 0.1° for $\epsilon = 3°$. Since $\delta\epsilon$ is small, we can expand the $\cot\epsilon'$ term in (13) to yield

$$\delta m(\epsilon, \phi) \simeq m_o(\epsilon) \cot\epsilon \left[1 - 10^{-6} N_s \csc^2\epsilon\right] \times [Z_n \cos\phi + Z_e \sin\phi] \tag{17}$$

The data used for this study were all obtained from elevation angles of 23.6° or greater (i.e., from an air mass of 2.5 or less). At this lowest elevation angle, the difference between ϵ and ϵ' is less than 3′, a value too small to affect our results. We include this correction only for the sake of generality and for use in "extrapolating" these results to greater air masses.

Gardner [1977] also developed a gradient correction. His expression and (17) are difficult to compare because this work uses gradients in the refractivity, while Gardner's work explicitly uses gradients in pressure and temperature. Water vapor gradients are not considered by Gardner because his correc-

tion was intended for laser (i.e., optical) tracking. However, one can compare the forms of the corrections. Both have the same azimuth dependence. Gardner explicitly approximates the no-gradient mapping function using cosecant, whereas we retain the general function $m_o(\epsilon)$. The expressions (16) and (17) should therefore be more accurate than Gardner's for low elevations, and in fact Gardner's correction has the wrong sign for low elevations [Davis, 1986]. Both expressions have two terms, with the first being positive and the second being negative. The elevation angle dependence of the second term is different because Gardner approximates more accurately the bending correction for higher atmospheric altitudes, where water vapor is present in minute amounts relative to surface values. Nevertheless, since here we are interested in propagation effects of water vapor located in the troposphere, (16) is adequate for our purposes.

ESTIMATING GRADIENT PARAMETERS

As we mentioned above, the most convenient quantities to examine are determinations of the equivalent zenith delay, which, in the absence of horizontal heterogeneities, are equal for different elevation angles. Let $\Delta L(\epsilon, \phi)$ be the wet delay determined from WVR data when it was pointing in the direction defined by the elevation angle ϵ and azimuth ϕ. Then the equivalent zenith delay $\Delta \check{L}^z$ is given by

$$\Delta \check{L}^z(\epsilon, \phi) = \Delta L(\epsilon, \phi)/m_o(\epsilon) \tag{18}$$

Using the results (8)–(17), (18) can be written as

$$\Delta \check{L}^z(\epsilon, \phi) = \Delta L^z + \cot\epsilon \left[1 - 10^{-6} N_s \csc^2 \epsilon\right] \times [\Xi_n \cos\phi + \Xi_e \sin\phi] \tag{19}$$

where $\vec{\Xi}$, the "delay gradient," is defined in Table 1. The integrals have been replaced by parameters as in (14) to indicate that one cannot solve for the gradient profile, but only its integrated value. This situation arises because the WVR measures only integrated quantities: see (1).

Given WVR determinations of the equivalent zenith delay, one could use (19) as a model and estimate the three parameters ΔL^z, Ξ_e, and Ξ_n. Examination of Figure 2 reveals immediately an inadequacy of this model. The original statement of the model (6) contained an explicit time dependence. That time dependence is implicit in (19), although, from examining Figure 2, it should be an explicit feature of the model. A simple way of adding time dependence in the model is to assume that each altitude has associated with it a constant wind velocity $\vec{v}(z)$. By replacing $\vec{x}$ in (6) with $\vec{x} - \vec{v}\Delta t$, the frozen turbulence hypothesis [e.g., Stull, 1988] is satisfied. With this assumption, the wind velocity and gradient are coupled to the change in (zenith) delay in an intuitive fashion. For example, if the refractivity field were blown over the site by winds from the direction of the positive gradient, the zenith delay would increase.

The form of (19) modified for the velocity term as above is

$$\Delta \check{L}^z(\epsilon, \phi, \Delta t) = \Delta L^z + \cot\epsilon \left[1 - 10^{-6} N_s \csc^2 \epsilon\right] [\Xi_n \cos\phi + \Xi_e \sin\phi] - 10^{-6} \Delta t \int_0^\infty dz\, \vec{\xi}(z) \cdot \vec{v}(z) \tag{20}$$

where Δt is the time from the reference epoch, that is, the epoch to which ΔL^z and $\vec{\Xi}$ are referred. Examination of (20) reveals that not only can one not solve for the wind profile, but one cannot separate the north and east components. In order to understand this last result, consider the following two situations for which (20) predicts no zenith delay changes in time: (1) $v_n = v_e = 0$, and (2) $\vec{\xi} \cdot \vec{v} = 0$. In the first case, the lack of wind causes no change in the zenith delay, regardless of the gradient. In the second case, the wind is blowing along the direction of zero gradient, so the wind gradient coupling causes no change in the zenith delay. Ishimaru [1972] discussed a method for determining wind speed from the ratio of amplitude spectra of received signals at two frequencies. Thus it may be possible to resolve the ambiguity by examining spectra of our brightness-temperature measurements.

The inclusion of time dependence therefore adds only one new estimable parameter, which we will call V_L (see Table 1):

$$\Delta \check{L}^z(\epsilon, \phi) = \Delta L^z + \cot\epsilon \left[1 - 10^{-6} N_s \csc^2 \epsilon\right] [\Xi_n \cos\phi + \Xi_e \sin\phi] + V_L \Delta t \tag{21}$$

The parameter V_L can be interpreted to be the time derivative of the zenith delay.

Figure 4*a* shows the same WVR data as Figure 3*a* (ASTRID only), along with the predicted values based on a least squares solution to the four-parameter model in (21). The estimated parameters are given in Table 2. Figure 4*b* shows the equivalent zenith delay residuals. A separate fit was performed for each of the two scans, so that (21) was extended over about 5 min of data. The rms residual was 1.2 mm for the earlier scan and 1.3 mm for later scan. (There are 26 observations in each scan.) The rms residual for a nongradient model, that is, a model with only a zenith delay and a zenith delay rate, was 1.7 mm for the earlier scan and 3.5 mm for the later scan. An F test for the significance of the gradient terms [Bevington, 1969] indicates that the additional gradient terms significantly improve χ^2 at better than the 99% level (based on χ^2 reduction).

For the data in Figure 5, we performed the same analysis as for Figure 4, except that the data from both scans were analyzed together, with only one set of parameters being estimated. For this analysis, the fit is significantly worse, with an rms residual for the two groups of 2.0 mm. The nongradient model yields an even poorer fit, 6.0 mm. The significantly larger rms residual and χ^2 for the residuals in Figure 5*b* imply that the model in (21) is inadequate for time periods longer

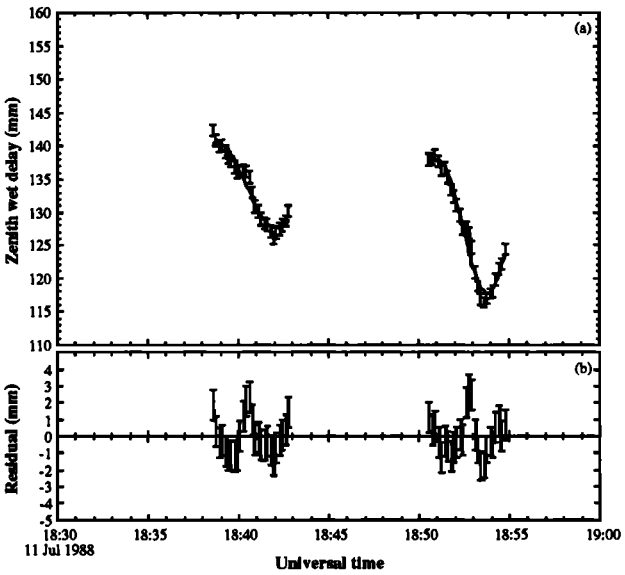

Fig. 4. (*a*) The azimuth scans from Figure 3, along with the four-parameter gradient model (see equation (21)). The values for the parameters were determined independently for each scan by a least squares adjustment. (*b*) Residuals to this fit. Note the scale change. The weighted root-mean-square (wrms) residual is 1.2 mm for the earlier scan ($\chi^2_\nu = 1.7$), and 1.3 mm for the later scan ($\chi^2_\nu = 2.1$). The combined wrms residual is 1.2 mm ($\chi^2_\nu = 1.9$).

than about 10 min because, as Figure 2 demonstrates, gradients can change significantly over that time. This inadequacy suggests a simple modification to (21):

$$\begin{aligned}\Delta\tilde{L}^z(\epsilon,\phi,\Delta t) &= \Delta L^z + V_L\Delta t \\ &+ \cot\epsilon\left[1 - 10^{-6}N_s\csc^2\epsilon\right] \\ &\times\left[\Xi_n\cos\phi + \Xi_e\sin\phi\right. \\ &\left.+ \dot{\Xi}_n\Delta t\cos\phi + \dot{\Xi}_e\Delta t\sin\phi\right] \qquad (22)\end{aligned}$$

The added parameters are the components of $\dot{\vec{\Xi}}$, the gradient rate.

Figures 6 and 7 show examples of WVR data and the resulting fits to (22) for different data sets. Figure 6 shows the same data presented previously. The combined fit using (22) gives the same weighted root mean square (wrms) residual as when then four-parameter model was fit separately for each scan. The estimated parameters for this fit are also shown in Table 2 ("solution *d*"). From this table it can be seen that, whereas the estimate of the gradient from the combined fit using the four-parameter model ("solution *c*") is approximately the average of the gradient from the two groups, when the six-parameter model is used, the gradient begins at the value for the first group and then increases at a rate of approximately 0.2 mm min^{-1}.

Figure 7 shows a case for which the WVR was performing neither simple azimuth scans nor simple elevation scans. In this case, the pattern within the data is difficult to interpret. From the residuals to a fit of (22) to these data, however, one can see that the hidden elevation, azimuth, and time dependencies are well modeled by (22). The wrms residual for these data is also 0.7 mm.

The model in (22) does not represent a full second-order Taylor expansion, and it does not satisfy the frozen turbulence hypothesis. A full second-order Taylor expansion would begin by adding a term $\vec{x}\cdot\Gamma\cdot\vec{x}$ to (6), where Γ is the second derivative tensor. In order to add the time dependence so as to satisfy the frozen turbulence hypothesis, this term would become $(\vec{x} - \vec{v}\Delta t)\cdot\Gamma\cdot(\vec{x} - \vec{v}\Delta t)$. When expanded, this second-order term would add not only the terms shown in (22), but terms proportional to $(\Delta t)^2$, $\cos^2\phi$, $\sin^2\phi$, and $\cos\phi\sin\phi$. Using a limited data set we have found that, for 30-min time spans, the estimates of the coefficients of these terms were highly correlated with each other and consequently possessed large uncertainties, without significantly improving the fit. One method for decreasing the uncertainties of the estimates would be to include more data by using longer time spans. We have found though that just as (6) broke down when we went to longer time spans, so the second-order Taylor expansion breaks down before most of these second-order terms

TABLE 2. Estimated Parameters for Scans of Figure 3

Solution	wrms Residual, mm	ΔL^z, mm	V_L, mm/min	$\lvert\vec{\Xi}\rvert$, mm	$\phi_{\vec{\Xi}}$, deg	$\lvert\dot{\vec{\Xi}}\rvert$, mm/min	$\phi_{\dot{\vec{\Xi}}}$, deg
a	1.2	135 ± 11	-0.8 ± 0.5	3.5 ± 0.5	121 ± 4	...	...
b	1.3	125 ± 11	1.5 ± 0.5	8.3 ± 0.5	120 ± 2	...	...
c	2.0	135 ± 2	-0.52 ± 0.02	5.0 ± 0.1	116 ± 2	...	...
d	1.2	135 ± 3	-0.45 ± 0.02	3.4 ± 0.2	122 ± 4	0.23 ± 0.02	99 ± 6

The solutions use the data from Figure 4*a* as follows: *a*: earlier group, four-parameter model (21); *b*: later group, four-parameter model; *c*: both groups together, four-parameter model; *d*: both groups together, six-parameter model (22).

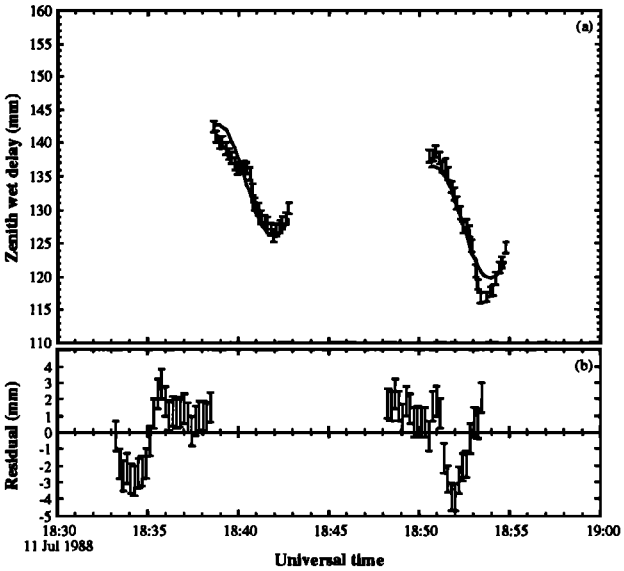

Fig. 5. (*a*) Same as Figure 4*a*, except a combined fit was performed. (*b*) Residuals to this fit. Note the scale change. The wrms residual is 2.0 mm ($\chi^2_\nu = 4.9$).

become significant. We interpret this result to mean that Taylor expansions are inadequate for representing the temporal variability of water vapor over the time necessary to determine adequately the higher-order terms, a result of the stochastic nature of water vapor variations [Tatarskii, 1961]. For time spans of up to 30 min, however, (22) has been adequate. That

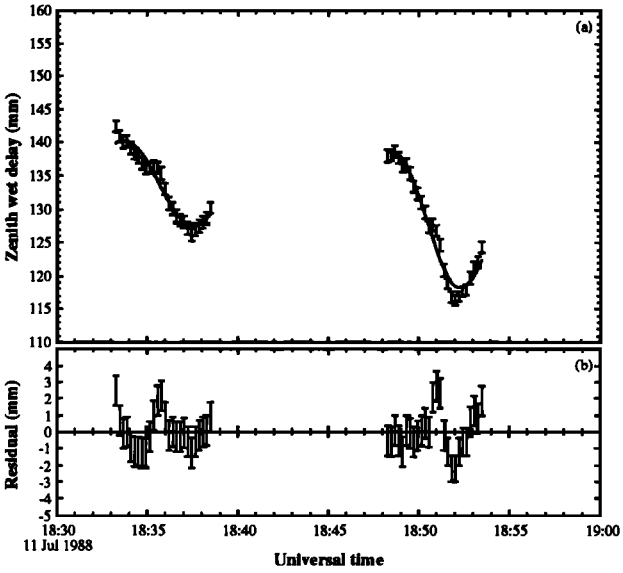

Fig. 6. (*a*) Same as Figure 5*a*, except the six-parameter model (22) was used. The solid line shows this model using the estimated parameters. (*b*) Residuals to this fit. Note the scale change. The wrms residual is 1.2 mm ($\chi^2_\nu = 1.8$).

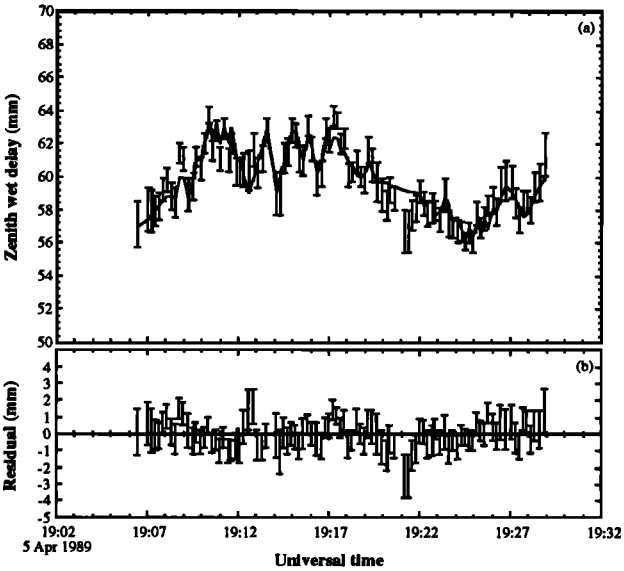

Fig. 7. (*a*) Equivalent zenith wet delay observations for a 30-min period on April 5, 1989. As with Figure 6, the solid line shows the calculated values using the fit to the six-parameter model. (*b*) Residuals. The wrms residual is 0.7 mm ($\chi^2_\nu = 0.9$).

(22) is not consistent with frozen flow is a consequence of our not being able to determine accurately coefficients of higher-order expansions. Thus we can neither confirm nor refute the frozen flow hypothesis with these WVR data.

STATISTICAL CHARACTERIZATION OF PARAMETERS

In order to obtain a better understanding of the gradients in the vicinity of the Onsala site, we undertook a large-scale analysis of ASTRID WVR data. For this study we chose to use all Onsala WVR data from 1988, the first year in which the WVR was often performing the azimuth scans described above. Unfortunately, no data were available for February through May, when the WVR was undergoing maintenance and some upgrading. Furthermore, no data were used when the WVR brightness temperatures indicated a columnar zenith liquid water content of 0.3 mm or greater, that is, during precipitation or heavy cloud cover.

The WVR data consist of sky brightness temperatures at both frequency bands. These sky brightness temperatures were calculated from the WVR's digital output using instrumental gains estimated from frequent tip curves; the determination of these gains was therefore potentially corrupted by the presence of gradients which were not taken into account in the analysis of the tip curves. The tip-curve data, however, were obtained in the four cardinal azimuths, so that the effects of constant gradients would average in the determinations of the instrumental gain. Furthermore, the values of the gains were averaged over several hours. Simple formulations of the effects of gradients have been preliminarily incorporated directly into

the models used for tip-curve analysis, but these algorithms were not used in the analysis of the data used here. In the future, we expect gradient models to be incorporated routinely into tip-curve analyses.

The gradient analysis code operated by grouping together all the WVR data within a user-defined time period (30 min for this study). The gains having been determined as described above, the two brightness temperatures for each WVR measurement were then combined using a site-specific algorithm [e.g., Johansson et al., 1987] to provide an estimate of the wet delay. The so-called "oxygen correction" [e.g., Davis, 1986] was not applied (although it was applied in the gain analysis). This term represents a correction of only 2–3 mm at zenith, is slowly varying, and will thus be absorbed by the zenith delay parameter in (22).

The equivalent zenith delay values obtained from the WVR data were then used to estimate the six parameters of (22). The program then searched for the first WVR observation beginning after the group of data used for this solution, and the process continued. In this manner, we obtained "independent" estimates of the six parameters approximately every 30 min. Some 30-min spans did not contain enough data to obtain a solution (due to cuts for high liquid content, for example).

A histogram of the resulting wrms residuals is shown in Figure 8. This distribution is somewhat broader than might be expected based on the average wrms residual, but the peak occurs at a somewhat smaller value (0.8–0.9 mm).

The monthly averages for the estimated parameters are indicated by the squares in Figures 9*a*–9*f*. The wrms variations about the average for each month are also plotted as triangles. (We will show the series of estimates for a few of the months below.) The gradient and gradient rate parameters are presented as magnitude and direction instead of as orthogonal components.

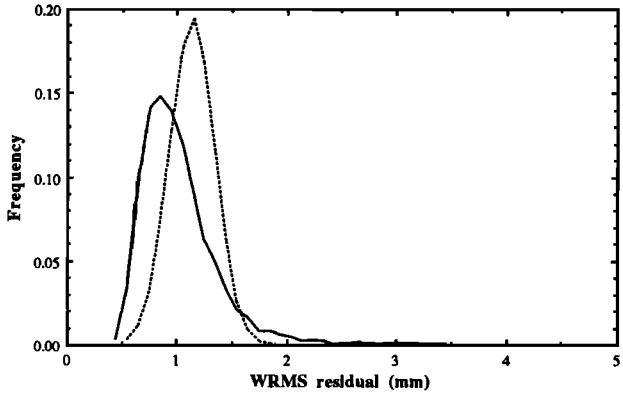

Fig. 8. Solid line denotes histogram of the 5812 wrms residuals for the fits to the six-parameter model. The bin width is 0.1 mm. Dashed line denotes theoretical prediction, based on the average (in a root-sum-square sense) wrms residual of 1.09 mm and assuming that 60 data were used for each fit.

As expected, the average wet zenith delays (Figure 9*a*) for the summer months are greater than for the fall and winter months. The monthly average wet delay rates (Figure 9*b*) are nearly zero. This also might be expected, since no long-term changes in water vapor are generally observed. (The summer/winter zenith delay changes, from Figure 9*a*, are about 80 mm, or ~0.0003 mm min^{-1} average, compared to the wrms scatter for the zenith wet delay rates of 0.10–0.15 mm min^{-1}.)

The gradient averages (Figure 9*c*), like the zenith delay averages, are larger in summer than winter. Unlike the average wet delay rate estimates, the average gradients are not negligible compared to their monthly variation. The wrms variability of the gradient azimuth (Figure 9*d*) is generally 70°–80°, although in January it was 52°. (The "average" directions were calculated by averaging sines and cosines of the azimuths in order to account for the 360° ambiguity of the gradient azimuth determination.) If the estimates of the gradient azimuths were uniformly distributed between 0° and 360°, the expected wrms variations about the average azimuth would be 103.9°. For several hundred independent estimates, the rms statistic, under the hypothesis of a uniform distribution and equally weighted estimates, is robust, with the 99% confidence limit being less than ±1°. (This limit is only approximate for our case, in which the estimates are not uniformly weighted and the averages were formed using a coherent sum described above.) We conclude that a uniform distribution between 0° and 360° does not describe our gradient azimuth estimates, and a preferred monthly direction, or range of directions, is indicated.

This conclusion is born out by Figure 10*a*. This plot is a polar histogram of gradient directions. The bin width is 30°, and only direction estimates with standard deviations of 10° or less are counted. The nonuniformity of the distribution of gradient directions is clearly apparent from this plot.

The statistical analysis of the gradient rate azimuths (Figure 9*f*) leads us to a different conclusion than that for the gradient azimuths. The monthly wrms values range from 96°–105°, roughly consistent with the scatter expected for a uniform distribution. Figure 10*b* is a polar histogram of the gradient rate estimates. Fewer gradient rate estimates meet our restriction of $\sigma < 10°$. The distribution of gradient rate azimuths is not peaked in a single direction as were the gradient azimuths, but two smaller peaks, in the bins for 30°–60° and 210°–240°, are visible. These bins are separated by 180°, indicating gradient rate vectors of opposite sign but in the same direction, leading to an elliptical form for the polar histogram.

Examples of individual parameter estimates for September and December are shown in Figures 11 and 12. The gradient rate azimuths seem fairly uniform, whereas a predominant direction is clearly visible for the gradient azimuths. This direction is 100°–150° (ESE–SE), in agreement with the histogram of Figure 10*a*.

DISCUSSION

What do the estimated gradient parameters tell us about gradients in the atmosphere? Thus far, we have avoided specific

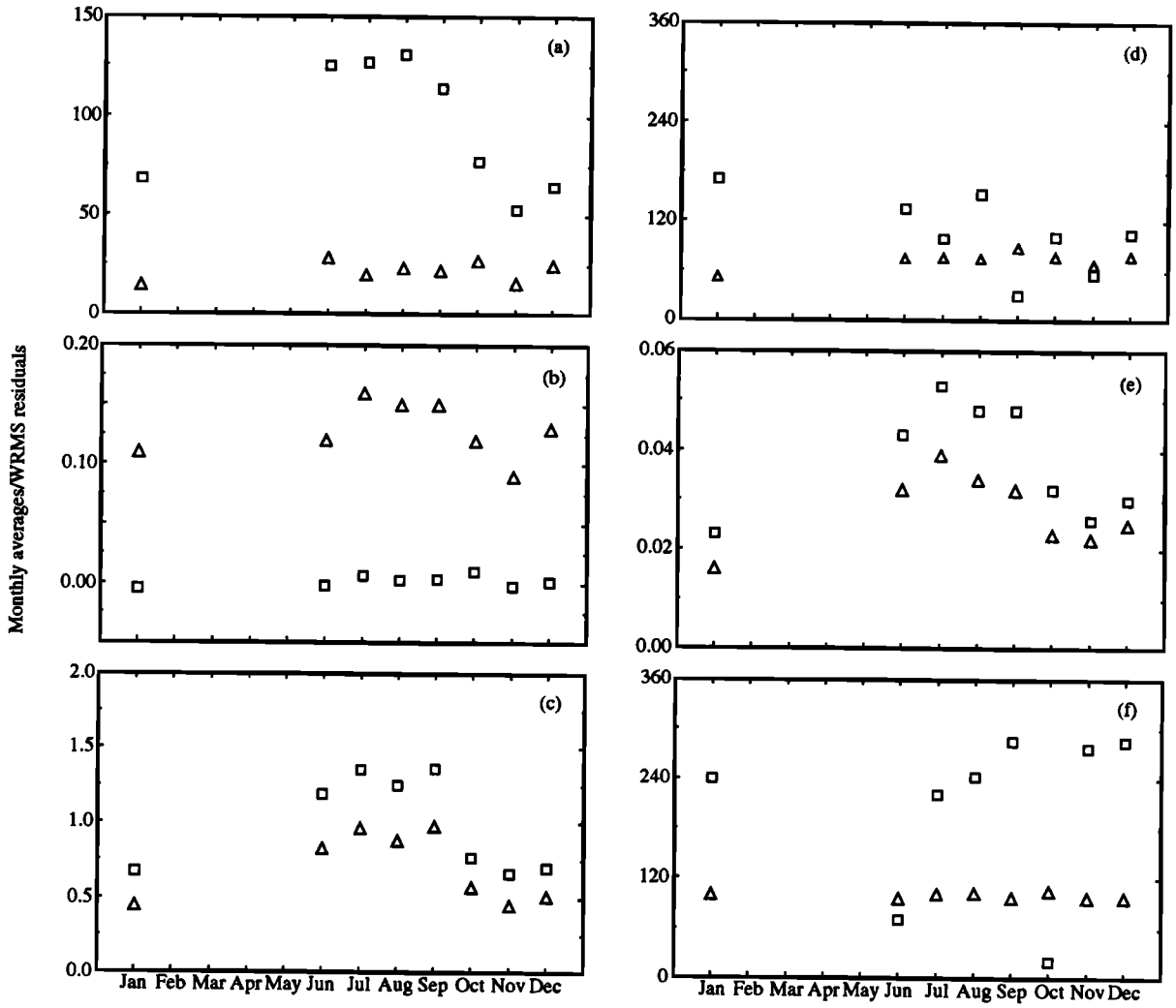

Fig. 9. Squares denote monthly averages for 1988 for the six parameters of the model (22). Triangles denote wrms residual about the mean. See text for estimation procedure. (*a*) Zenith delay, mm. (*b*) Zenith delay rate, mm min^{-1}. (*c*) Zenith delay gradient, mm. (*d*) Azimuth of the zenith delay gradient, degrees. (*e*) Zenith delay gradient rate, mm min^{-1}. (*f*) Azimuth of the zenith delay gradient rate, degrees.

models for the profiles of water vapor and temperature. Because the WVR is sensitive to the integrated refractivity, one is unable to determine uniquely these profiles from our data. Let us, for investigative purposes, examine a water vapor refractivity field given by

$$N_v(\vec{x}, z) = N_o(z)\left[1 + \vec{\alpha} \cdot \vec{x}\right] \tag{23}$$

where $N_o(z)$ is the refractive index at $\vec{x} = 0$, and $\vec{\alpha}$ is a constant vector. From (23), $\vec{\alpha}$ and the refractivity gradient $\vec{\xi}$ are related by

$$\vec{\xi}(z) = N_o(z)\vec{\alpha} \tag{24}$$

In other words, we are assuming that the gradient scales linearly with refractivity. From Table 1, the delay gradient $\vec{\Xi}$ is given by

$$\vec{\Xi} = 10^{-6}\int_0^\infty dz\; z\; \vec{\xi}(z)$$
$$= 10^{-6}\vec{\alpha}\int_0^\infty dz\; z\; N_o(z) \tag{25}$$

In order to compute the integral in (25), we will assume a form for the refractivity which represents an "average" profile:

$$N_o(z) = N_s e^{-z/H} \tag{26}$$

where H is the water vapor scale height, usually found to be

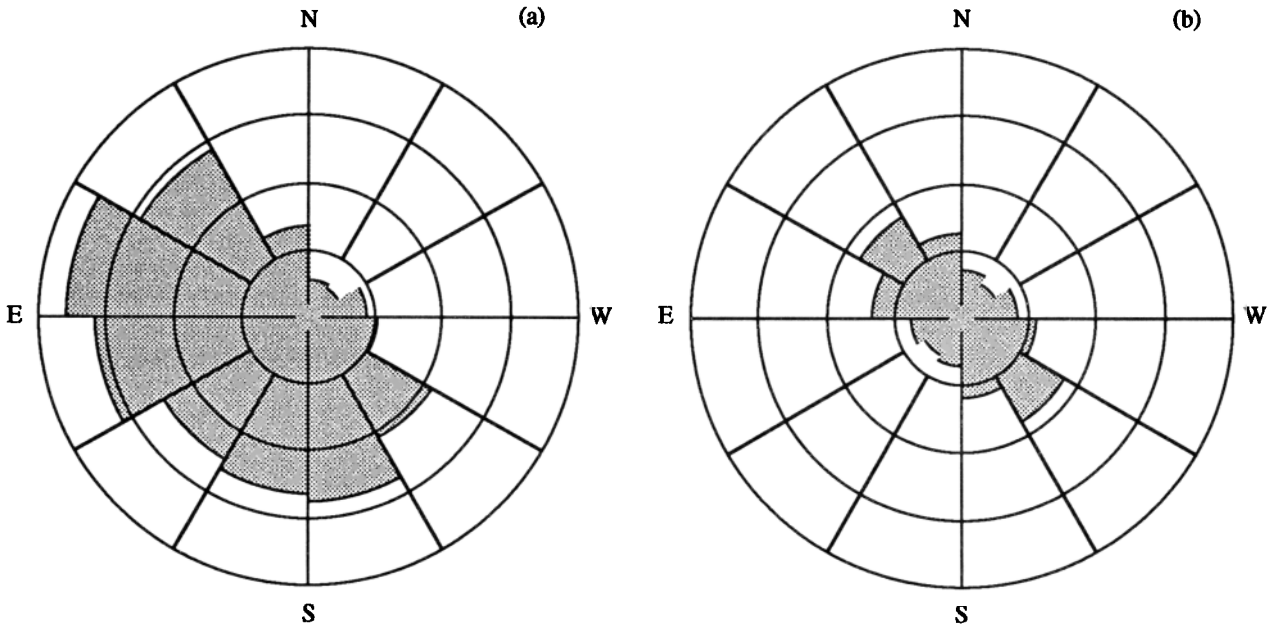

Fig. 10. Polar histograms of azimuth angles for estimated (*a*) gradient and (*b*) gradient-rate parameters. For both plots, the bin width is 30°, and only estimates with standard deviations of less than 10° are considered. The outer rings represent 400 binned samples.

1–2 km. Using the profile in (26), one can easily compute the integral in (25). The quantity of interest to us is the refractivity gradient, which, from (24)–(26), is

$$\vec{\xi}(z) = 10^6 \frac{\vec{\Xi}}{H^2} e^{-z/H} \tag{27}$$

From the statistical analysis of the previous section, the average estimated value for $|\vec{\Xi}|$ at the Onsala site was approximately 1 mm, with the largest value being approximately 8 mm. For a scale height of 1–2 km, the value of the average refractivity gradient at $z = 0$ is therefore 0.25–1.00 N km^{-1}. The summer time values are about 20% larger than this average, the fall/winter values 20% smaller. The 95% value (i.e., the value which is exceeded only 5% of the time) for summer is 1.0–3.9 N km^{-1}, for winter 0.6–2.3 N km^{-1}. These values are probably underestimates of the refractivity gradient near the surface, because the model (23) on which they are based assumes that the gradient direction is constant with altitude. If this assumption is false, a larger surface refractivity is required to integrate to the same amplitude.

Blanchetiere-Ciarletti et al. [1989] determined refractivity gradients using an airborne sensor package, flying at an altitude of 100–300 m above the ground. They measured local gradients at this altitude of up to 4 N km^{-1} over a 5 km path. They also detected 10 N km^{-1} "waves" of ~500 m wavelength associated with wind variations.

Gradients in temperature determined by Gardner [1977] imply wet radio-refractivity gradients, for constant water vapor pressure, of ~0.01 N km^{-1}. These temperature gradients were determined by measurements obtained from a network of radiosondes with closest spacing ~100 km. Similarly, Elgered et al. [1990] used surface meteorological data obtained ~100 km apart and determined temperature gradients as high as 0.1 K km^{-1} (corresponding to wet N gradients of 0.06 N km^{-1} for constant surface pressure). However, Elgered et al. [1990] used 11,000 points to determine a distribution, and by far the bulk of the points indicated gradients of less than 0.03 N km^{-1}. Thus local wet refractivity gradients, to which this work and the work of Blanchetiere-Ciarletti et al. are sensitive, can be several orders of magnitude larger than gradients inferred from temperature differences over 100-km distance scales. Our concentration on temperature gradients, rather than gradients in humidity, arises from our observation that there can be significant gradients in the wet delay during periods of little change in the wet delay.

Treuhaft and Lanyi [1987] calculated statistics for zenith delay variations. These calculations were based on the wet refractivity varying according to Kolmogorov turbulence theory [Tatarskii, 1961]. Treuhaft and Lanyi calculated the rms variation of zenith delay rate as a function of time over which the rate is to be averaged, to which our estimates of zenith delay variations may be compared. From their Figure 5, for an 1800-s interval the rms zenith delay rate is approximately 10^{-14} s s^{-1}. The units arise because Treuhaft and Lanyi refer to the delay in units of time. From our Figure 9, the wrms zenith delay rate parameter is approximately 0.12 mm min^{-1}, or 0.7×10^{-14} s s^{-1}. The uncertainty in the Treuhaft and Lanyi value is at least 30% due to the uncertainty in the nor-

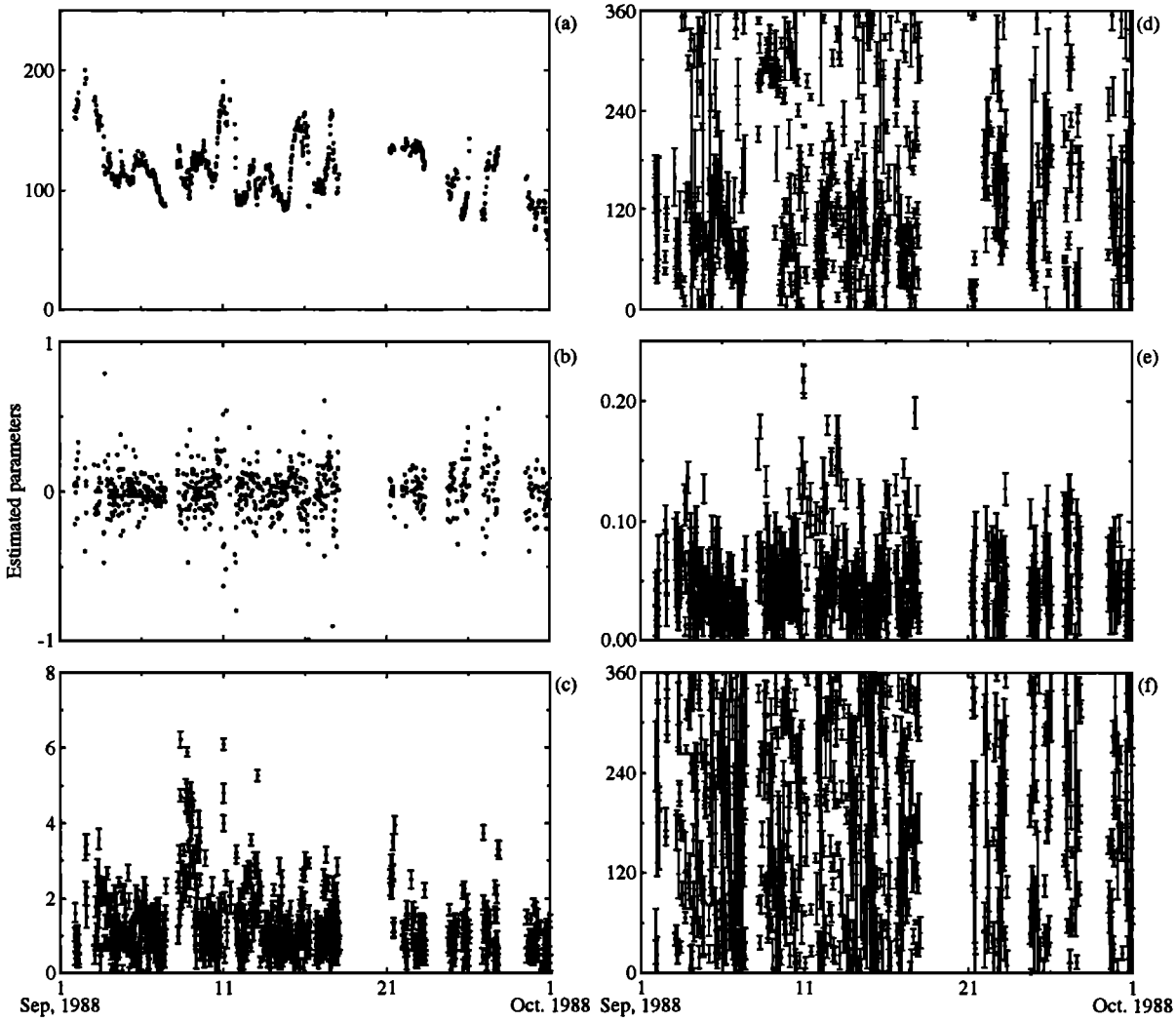

Fig. 11. Individual estimates of the six parameters of (22) for September 1988. Gaps in the data sequence are due mainly to precipitation or to the WVR performing an observation schedule inappropriate for estimating gradient parameters. See caption to Figure 9 for a description of the parameters and units.

malizing constant, and the monthly variability of the wrms zenith delay rate parameter is also about 30%, from Figure 9.

In (8) and thereafter, we neglected the difference in ray paths for the gradient and no-gradient cases. In other words, we assumed that the surfaces of constant refractivity were perpendicular to the zenith direction. In fact, at any point in space the normal to the refractivity surface and the zenith direction form an angle $\delta\epsilon_N$ given by

$$\tan(\delta\epsilon_N) = \frac{|\partial N_T/\partial x_h|}{|\partial N_T/\partial z|} \tag{28}$$

where N_T is the total refractivity, and x_h is the horizontal coordinate in the direction of the horizontal refractivity gradient. If one assumes that any horizontal gradient in the refractivity is due to the wet component and that the variation of the total refractivity can be described by an exponential decay with scale height H_T (usually taken to be ~7.5 km), then (28) is

$$\tan(\delta\epsilon_N) = \frac{\xi H_T}{N_T} \tag{29}$$

Using N_T = 300 N and ξ = 0.1–1 N km^{-1} (from above), we find a value for $\delta\epsilon_N$ of 0.1°–1.4°.

The effect on refraction of these tilted layers can be calculated from (16). A ray traveling in the direction of the gradient is refracted an extra amount $\delta(\delta\epsilon)$, given by

$$\delta(\delta\epsilon) = 10^{-6} N_T \csc^2\epsilon \quad \delta\epsilon_N \tag{30}$$

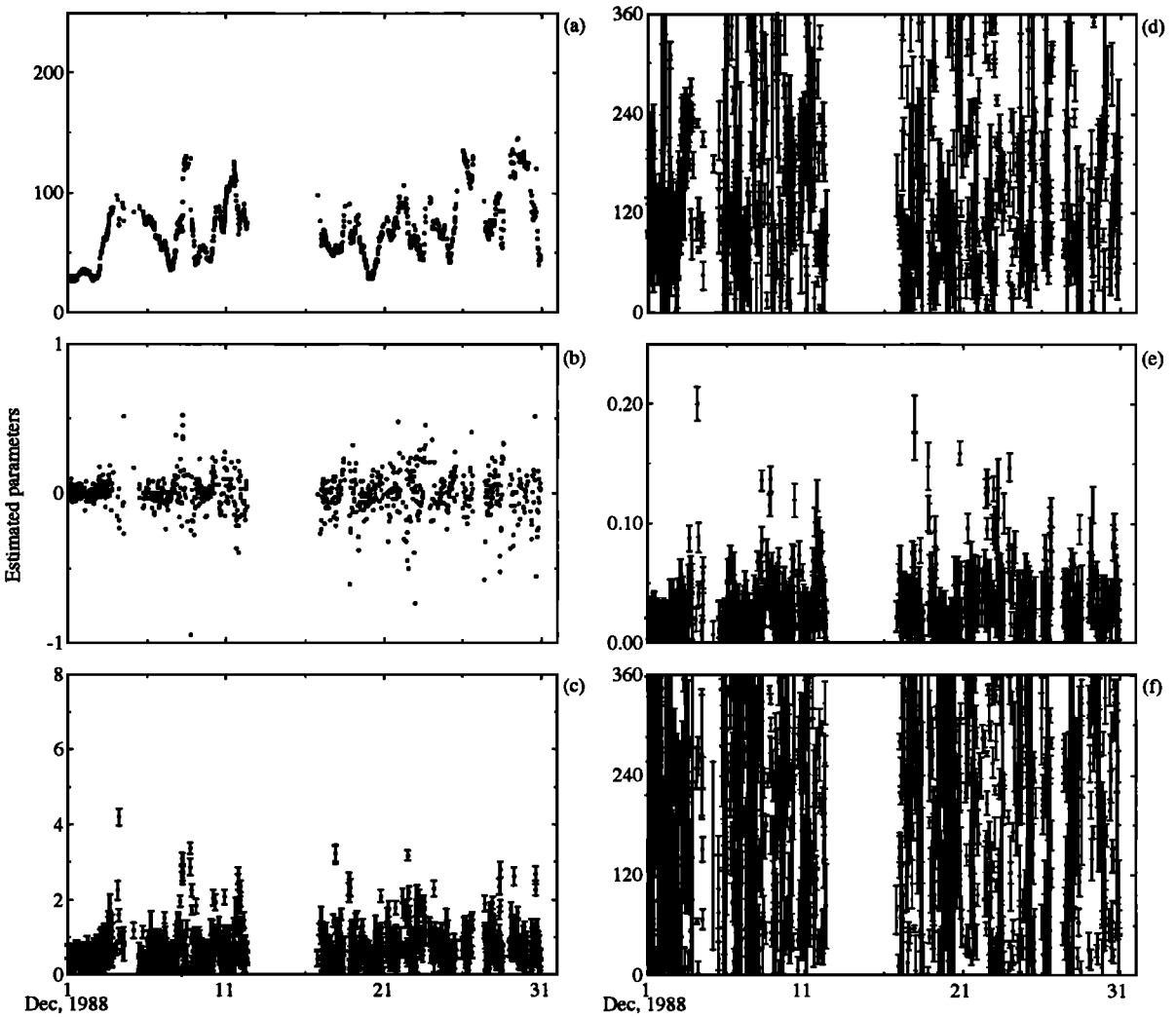

Fig. 12. Individual estimates of the six parameters of (22) for December 1988. Gaps in the data sequence are due mainly to precipitation or to the WVR performing an observation schedule inappropriate for estimating gradient parameters. See caption to Figure 9 for a description of the parameters and units.

The overall positive sign for $\delta(\delta\epsilon)$ in (30) results from the layers being tilted "backwards" for a ray traveling in this direction. Using the values for N_T and the maximum value for $\delta\epsilon_N$ from above, this gives a value for $\delta(\delta\epsilon)$ of

$$\delta(\delta\epsilon) = 1.5'' \csc^2 \epsilon \tag{31}$$

For example, a "zenith" ray is refracted by at most 2″, whereas a ray at elevation angle 20° is refracted by at most an extra 13″, for a path length error of 1 mm out of a total propagation delay of ~6.7 m.

CONCLUSION

We used data from a ground-based water vapor radiometer (WVR) to estimate horizontal gradient parameters in a simple model for the spatial and temporal variation of the wet refractivity. Because the WVR data are expressions of the integrated water vapor along a line of site, these estimates cannot be used to determine the refractivity gradients at any specific altitude. However, using a simple exponential vertical profile for the wet refractivity gradient, the average calculated horizontal water vapor N gradients are of the order of 0.1–1 N km^{-1}. This value is much larger than that determined by others by averaging over large (~100-km) distances. This result implies that for applications requiring local gradients (such as propagation delay models for geodetic studies with radio-interferometry), the use of meteorological data from widely separated stations is inadequate, although we have not undertaken a study to determine if large-scale and small-scale gradients are correlated.

The simple model we developed for the temporal and spatial variations of the wet refractivity is adequate for times up to 30 min and elevation angles above 23.6°. (The model is not limited to this range of elevation angles in principle, but none of our data were acquired below this elevation angle.) Tests show that the model is inadequate for longer times, even if no gradients are present, because of the complicated stochastic like temporal behavior of the wet atmosphere. Nevertheless, our ability to fit the radiometer data implies that on these shorter timescales the local structure of the wet atmosphere can be described by a simple model, at the level of the rms residual of the WVR zenith delay estimates (~1 mm).

For the WVR data presented here, the estimates of the gradient and gradient rate vectors exhibit preferred azimuths. We have not attempted to speculate as to the cause of these preferences, leaving this instead to a more detailed study of local refractive index variations. Since the Onsala WVR is located within 200 m of the sea coast, it might be expected that the presence of the ocean and attendant sea breezes play a role in forming prevailing gradients of temperature and humidity. However, since this site is on a peninsula, the sea-land-atmosphere interactions could be complex, and so we have postponed interpretation of the azimuths until more data are available.

Davis [1992] showed that atmospheric turbulence can affect estimates of gradient parameters from WVR data. That the WVR does not obtain an instantaneous "snapshot" of the sky means that the frozen field passing over the site can appear as prevailing gradients. However, the calculated gradients due to this effect were less than 1 mm.

Acknowledgments. This work was supported by the Smithsonian Institution, NSF grant EAR-9105502, and by National Aeronautics and Space Administration grant NAG5-538 and contract NAS5-30543. The research using water vapor radiometry at the Onsala Space Observatory is supported by the Swedish Natural Science Research Council (which also provided visiting scientist funds for J.L.D.), the Hasselblad Foundation, and the European Space Agency. We would like to thank I. Shapiro and D. Lebach for their comments, and two anonymous referees for their reviews.

REFERENCES

Bean, B. R., and E. J. Dutton, *Radio Meteorology, NBS Monograph Ser.*, vol. 92, 435 pp., U.S. Government Printing Office, Washington, D.C., 1966.

Bevington, P. R., *Data Reduction and Error Analysis for the Physical Sciences*, 336 pp., McGraw-Hill, New York, 1969.

Blanchetiere-Ciarletti, V., J. Lavergnat, M. Sylvain, and A. Weill, Experimental observation of horizontal refractivity gradients during periods of multipath propagation, *Radio Sci.*, *24*, 705–724, 1989.

Boudouris, G., On the index of refraction of the air, the absorption and dispersion of centimeter waves by gasses, *J. Res. Natl. Bur. Stand.*, *67D*, 631–684, 1963.

Chandrasekhar, S., *Radiative Transfer*, 393 pp., Dover, New York, 1960.

Davis, J. L., Atmospheric propagation effects on radio interferometry, *Tech. Rep. AFGL-TR-86-0243*, 276 pp., Air Force Geophys. Lab., Hanscom AFB, Mass., 1986.

Davis, J. L., The effect of turbulence on atmospheric gradient parameters estimated from ground-based radiometric and space geodetic measurements, *Geophys. Res. Lett.*, *19*, 2183–2186, 1992.

Davis, J. L., T. A. Herring, I. I. Shapiro, A. E. E. Rogers, and G. Elgered, Geodesy by radio interferometry: Effects of atmospheric modeling errors on estimates of baseline length, *Radio Sci.*, *20*, 1593–1607, 1985.

Dixon, T. H., and S. Kornreich Wolf, Some tests of wet tropospheric calibration for the CASA Uno Global Positioning System experiment, *Geophys. Res. Lett.*, *17*, 203–206, 1990.

Elgered, G., Tropospheric wet path-delay measurements, *IEEE Trans. Antennas Propag.*, *AP-30*, 502–505, 1982.

Elgered, G., J. M. Johansson, and B. O. Rönnäng, Characterizing atmospheric water vapour fluctuations using microwave radiometry, *Res. Rep. 165*, 400 pp., Chalmers University of Technology, Göteborg, Sweden, 1990.

Elgered, G., J. L. Davis, T. A. Herring, I. I. Shapiro, Geodesy by radio interferometry: Water vapor radiometry for estimation of the wet delay, *J. Geophys. Res.*, *96*, 6541–6555, 1991.

Gardner, C. S., Correction of laser tracking data for the effects of horizontal refractivity gradients, *Appl. Opt.*, *16*, 2427–2432, 1977.

Herring, T. A., J. L. Davis, I. I. Shapiro, Geodesy by radio interferometry: The application of Kalman filtering to the analysis of very long baseline interferometry data, *J. Geophys. Res.*, *95*, 12,561–12,581, 1990.

Ishimaru, A., Temporal frequency spectra of multifrequency waves in turbulent atmosphere, *IEEE Trans. Antennas Propag.*, *AP-20*, 10–19, 1972.

Johansson, J. M., A Study of precise position measurements using space geodetic systems, *Tech. Rep. 229*, 146 pp., Chalmers University of Technology, Göteborg, Sweden, 1992.

Johansson, J. M., G. Elgered, and J. L. Davis, Geodesy by radio interferometry: Optimization of wet path delay algorithms using microwave radiometer data, *Res. Rep. 152*, 50 pp., Chalmers University of Technology, Göteborg, Sweden, 1987.

Käll, B. A., Estimating horizontal gradients in the wet delay using microwave radiometry, M.S. thesis, 37 pp., Chalmers University of Technology, Göteborg, Sweden, 1991.

Kuehn, C. E., G. Elgered, J. M. Johansson, T. A. Clark, and B. O. Rönnäng, A microwave radiometer comparison and its implication for the accuracy of wet delays, in *Space Geodesy and Geodynamics, Geodyn. Ser.*, vol. 23, edited by D. Smith and D. Turcotte, AGU, Washington, D.C., in press, 1993.

Liebe, H. J., An updated model for millimeter wave propaga-

tion in moist air, *Radio Sci.*, *20*, 1069–1089, 1985.

Liebe, H. J., A contribution to modeling atmospheric millimeter-wave properties, *Frequenz*, *41*, 31–36, 1987.

Liebe, H. J., MPM—An atmospheric millimeter-wave propagation model, *Int. J. Infrared Millimeter Waves*, *10*, 631–650, 1989.

Liebe, H. J., G. A. Hufford, and T. Manabe, A model for the complex permittivity of water at frequencies below 1 THz, *Int. J. Infrared Millimeter Waves*, *12*, 659–675, 1991.

Reber, E. E., and J. R. Swope, On the correlation of the total precipitable water in a vertical column and absolute humidity at the surface, *J. Appl. Meteorol.*, *11*, 1322–1325, 1972.

Resch, G. M., Water-vapor radiometry in geodetic applications, in *Geodetic Refraction*, edited by F. K. Brunner, pp. 53–84, Springer-Verlag, New York, 1984.

Staelin, D. H., Measurements and interpretation of the microwave spectrum of the terrestrial atmosphere near 1-centimeter wavelength, *J. Geophys. Res.*, *71*, 2875–2881, 1966.

Stull, R. B., *An Introduction to Boundary Layer Meteorology*, Kluwer Academic, Norwell, Mass., 666 pp., 1988.

Tatarskii, V. I., *Wave Propagation in a Turbulent Medium*, translated by R.A. Silverman, McGraw-Hill, New York, 1961.

Treuhaft, R. N., and G.E. Lanyi, The effect of the dynamic wet troposphere on radio interferometric measurements, *Radio Sci.*, *22*, 251–265, 1987.

Wu, S. C., Optimum frequencies of a passive microwave radiometer for tropospheric path-length correction, *IEEE Trans. Antennas Propag.*, *AP-27*, 233–239, 1979.

J. L. Davis, Harvard-Smithsonian Center for Astrophysics, 60 Garden St., Mail Stop 42, Cambridge, MA 02138.

G. Elgered, Onsala Space Observatory, Chalmers University of Technology, S-43900 Onsala, Sweden.

C. E. Kuehn, Code 926.9, Interferometrics, Inc., NASA Goddard Space Flight Center, Greenbelt, MD 20771-0001.

A. E. Niell, Haystack Observatory, NEROC, Westford, MA 01886.